Factor VIII alters tubular organization and functional properties of von Willebrand factor stored in Weibel-Palade bodies

*Eveline A. M. Bouwens,[1,2] *Marjon J. Mourik,[3] Maartje van den Biggelaar,[1] Jeroen C. J. Eikenboom,[4] Jan Voorberg,[1,5] Karine M. Valentijn,[3] and Koen Mertens[1,2]

[1]Department of Plasma Proteins, Sanquin Research, Amsterdam, The Netherlands; [2]Department of Pharmaceutics, UIPS, Utrecht University, Utrecht, The Netherlands; [3]Department of Molecular Cell Biology, Leiden University Medical Center, Leiden, The Netherlands; [4]Department of Hematology and Thrombosis and Hemostasis, Leiden University Medical Center, Leiden, The Netherlands; and [5]Landsteiner Laboratory of AMC and Sanquin, University of Amsterdam, Amsterdam, The Netherlands

In endothelial cells, von Willebrand factor (VWF) multimers are packaged into tubules that direct biogenesis of elongated Weibel-Palade bodies (WPBs). WPB release results in unfurling of VWF tubules and assembly into strings that serve to recruit platelets. By confocal microscopy, we have previously observed a rounded morphology of WPBs in blood outgrowth endothelial cells transduced to express factor VIII (FVIII). Using correlative light-electron microscopy and tomography, we now demonstrate that FVIII-containing WPBs have disorganized, short VWF tubules. Whereas normal FVIII and FVIII Y1680F interfered with formation of ultra-large VWF multimers, release of the WPBs resulted in VWF strings of equal length as those from nontransduced blood outgrowth endothelial cells. After release, both WPB-derived FVIII and FVIII Y1680F remained bound to VWF strings, which however had largely lost their ability to recruit platelets. Strings from nontransduced cells, however, were capable of simultaneously recruiting exogenous FVIII and platelets. These findings suggest that the interaction of FVIII with VWF during WPB formation is independent of Y1680, is maintained after WPB release in FVIII-covered VWF strings, and impairs recruitment of platelets. Apparently, intracellular and extracellular assembly of FVIII-VWF complex involves distinct mechanisms, which differ with regard to their implications for platelet binding to released VWF strings. (*Blood*. 2011; 118(22):5947-5956)

Introduction

Weibel-Palade bodies (WPBs) are secretory organelles specific for vascular endothelial cells with a typical elongated shape of 100 to 200 nm in diameter and up to 5 μm in length.[1] These organelles are characterized by striations running along the longitudinal axis consisting of condensed von Willebrand factor (VWF). Stimulation with agonists, such as thrombin and epinephrine, releases VWF to arrests bleeding by recruiting blood platelets to sites of vascular perturbation.[2] VWF is synthesized as a prepropolypeptide of 2813 residues that is cleaved into a propeptide (D1-D2) and mature VWF monomer (D′-D3-A1-A2-A3-D4-B1-B2-B3-C1-C2-CK) of approximately 250 kDa.[3] VWF forms multimers through C- and N-terminal disulfide linkage.[4-6] Multimers assemble into long, slightly twisted tubules that determine the typical cigar-shaped appearance of WPBs.[7-9] On fusion of WPBs with the plasma membrane, VWF tubules are exposed to physiologic pH. This results in rapid disassembly of VWF tubules, which is presumably triggered by dissociation of propeptide from D′-D3 regions at neutral pH.[8,10] The released VWF multimers assemble into extended string-like structures on the surface of endothelial cells onto which platelets adhere.[10-12] The tubular organization of VWF is thought to be essential for orderly secretion of long VWF strings without tangling.[13]

Besides recruiting platelets to sites of vascular damage, VWF functions as a chaperone for factor VIII (FVIII), a cofactor for activated factor IX in the factor Xase complex. It is thus far unclear where FVIII and VWF associate, but complex formation with VWF significantly increases circulation time of FVIII.[14] The FVIII-VWF complex is sustained through interactions of the FVIII light chain (a3-A3-C1-C2) with the D′-D3 region on VWF. The acidic a3 region (residues 1649-1689) harbors a high-affinity binding site that is removed during proteolytic activation of FVIII.[15] Loss of the sulfated tyrosine at position 1680 in this a3 region results in impaired complex formation with VWF.[16] FVIII is mostly synthesized in the liver, although emerging evidence demonstrates that FVIII can also be produced in other tissues. For instance, although liver transplantation in hemophilic recipients can correct circulating FVIII levels, transplantation does not restore the FVIII pool released after desmopressin treatment.[17] This indicates that there should be at least one additional extrahepatic source for FVIII.[18]

Several groups reported recently that subsets of endothelial cells exist that synthesize FVIII and store it with VWF in WPBs.[19-22] Previously, it was demonstrated that overexpression of FVIII in endothelial cells results in FVIII targeting to WPBs.[23-26] The targeting signal for FVIII sorting to WPBs is currently unclear, although the typical high-affinity interaction with VWF seems not required.[25,26] Interestingly, WPBs containing FVIII do not have their characteristic elongated shape but appear as rounded vesicles.[25,27] The mechanism behind this change in morphology is

Submitted May 18, 2011; accepted September 16, 2011. Prepublished online as *Blood* First Edition paper, September 22, 2011; DOI 10.1182/blood-2011-05-355354.

*E.A.M.B. and M.J.M. contributed equally to this study.

The online version of this article contains a data supplement.

The publication costs of this article were defrayed in part by page charge payment. Therefore, and solely to indicate this fact, this article is hereby marked "advertisement" in accordance with 18 USC section 1734.

poorly understood, and the effect of these alterations on functional properties of both FVIII and VWF is unknown. The aim of the present study was therefore to determine the intracellular and extracellular effects of FVIII costorage in WPBs. WPB morphology was analyzed using electron microscopy, and the functional implications were assessed by flow experiments, with particular reference to formation of VWF strings, platelet recruitment, and association with VWF.

Methods

Materials

All chemicals used were of analytical grade. The μ-slide I 0.4 Luer ibiTreat flow chambers were from Ibidi. Engraved glass-bottom dishes were from MatTek. Human serum albumin (CeAlb) was from Sanquin. 4,6-Diamidino-2-phenylindole and anti-GFP were obtained from Invitrogen. EGM-2 bullet kit was from Lonza Walkersville. Collagen type 1 rat tail was from BD Biosciences. Peroxidase-labeled polyclonal rabbit anti–human VWF antibody was from Dako Denmark. Tissue culture flasks, multidishes, and microtiter plates (Maxisorp) were from Nunc.

Transduction of BOECs

Lentiviral vector pLV-CAG-FVIII-GFP has been described before.[24] B domain deleted FVIII-YFP with a Y1680F point mutation in pcDNA3.1(+) was constructed as described.[26] The LV-CAG-FVIII-YFP Y1680F plasmid was created by replacing fragment *NheI-Xho*I from pLV-CAG-FVIII-GFP for the corresponding fragment of the pcDNA3.1(+)FVIII-YFP Y1680F. Production of viral vectors, blood outgrowth endothelial cell (BOEC) isolation, and transduction with the viral vectors have all been described elsewhere.[24]

CLEM and electron tomography

BOECs expressing FVIII-GFP were grown on collagen-coated engraved glass-bottom Petri dishes (MatTek), and correlative light and electron microscopy (CLEM) was performed as previously described.[28] Briefly, confluent cells were fixed with 3.7% paraformaldehyde (PFA) in PBS for 30 minutes at 4°C and counterstained with 4,6-diamidino-2-phenylindole. After imaging of nuclear staining and FVIII-GFP fluorescence with a Leica SP5 confocal microscope, the cells were fixed for electron microscopy with 2% glutaraldehyde in cacodylate buffer (0.1M sodium cacodylate, pH 7.4) and processed for transmission electron micrography (TEM) as previously described.[9] Briefly, cells were postfixed for 1 hour with 1% osmium tetroxide in cacodylate buffer and for 30 minutes in 1% tannic acid in cacodylate buffer. The samples were then dehydrated in ethanol (70%-100%) and embedded in Epon using one-beam capsule filled with Epon, which was placed on the cell layer at the region of the engraved grid where the fluorescence imaging was performed. Epon was polymerized at 60°C overnight. To detach the capsule from the glass coverslip, the Petri dish was placed repeatedly on liquid nitrogen and hotplate. Thin sections (120 nm) were placed on a 1-slot grid coated with Formvar and carbon, counterstained in 7% uranyl acetate and Reynolds lead citrate, and viewed with a Tecnai 12 transmission electron microscope at 120 kV equipped with a 4kx4k CCD camera (Model Eagle; Fei) as described before.[28] After finding correlated structures, protein-A gold (10 nm) was applied to the grids and used as fiducial marker for electron tomography. Double-tilt series from −60° to +60° were collected at a 1° interval using the Serial EM package.[29] Three-dimensional reconstructions were generated using the IMOD package.[30]

Immunogold labeling of cryosections

FVIII-GFP-transduced BOECs were fixed with 2% PFA and 0.2% glutaraldehyde in PHEM buffer (240mM PIPES, 100mM HEPES, 40mM EGTA, and 8mM $MgCl_2$, pH 6.9) for 2 hours at 4°C and stored in 0.5% PFA in PHEM buffer until processing for immunogold labeling as previously described.[31] Briefly, cells were scraped from the Petri dish, collected into an Eppendorf tube, and pelleted by gentle centrifugation. Thereafter, the cell pellet was carefully resuspended into warm (37°C) gelatin and quickly pelleted. Gelatin was then let to set and harden on ice, and small blocks of 1 mm^3 were cut with a razor blade and impregnated with 2.3M sucrose in PBS overnight at 4°C. Thereafter, the blocks were mounted on a pin using a drop of 2.3M sucrose and snap frozen in liquid nitrogen. The blocks were stored in liquid nitrogen until sectioning. Cryosections of 90 nm were collected in a mixture (volume/volume) of 2.3M sucrose and 2% methylcellulose in double-distilled H_2O, deposited on copper grids and stored at 4°C until labeling. Before labeling, the sections were warmed up on hard 1% gelatin at 37°C for 20 minutes. Grids were then deposited on a drop of PBS-"Gly" buffer (0.15% glycine, 0.1% BSA in PBS) to block nonspecific binding 4 times for 1 minute. Thereafter, the sections were labeled with a rabbit anti-GFP (Invitrogen) and indirectly with 15 nm protein A-gold particles (provided by the laboratory of Dr J. Klumperman, Utrecht Medical Center, Utrecht, The Netherlands) in PBS, 1% BSA. After fixation in 1.5% glutaraldehyde in PBS to block the free rabbit antibody from the first incubation step, the sections were labeled with rabbit anti-VWF (Dako Denmark), followed by incubation with 10 nm protein A-gold particles. Rinsing steps were performed in between using PBS-"Gly" buffer. The sections were contrasted and embedded in a mixture of uranylacetate-methylcellulose. As controls, anti-VWF or anti-GFP was omitted to rule out nonspecific binding of protein-A gold. In addition, to rule out masking effects, the labeling was performed in reverse order (ie, anti-VWF before anti-GFP). Acquisition of electron micrographs was performed on a Tecnai 12 transmission electron microscope mentioned in "CLEM and electron tomography."

VWF multimer analysis

Conditioned medium from nontransduced, FVIII-YFP-transduced and FVIII-YFP Y1680F-transduced BOECs was collected after 5 days of culture. Unstimulated cells were scraped and lysed in TBS, 1% Nonidet P40 supplemented with 10mM benzamidine and one protease inhibitor cocktail tablet per 50 mL (Roche Diagnostics) at 4°C for 30 minutes. Lysate was spun down at 16 000*g* and 4°C for 5 minutes, after which the pellet was discarded. To measure regulated exocytosis of WPBs, BOECs were washed twice with PBS and stimulated with SF medium supplemented with 50 ng/mL phorbol 12-myristate 13-acetate for 1 hour. Collected medium was centrifuged for 10 minutes at 10 000*g*, supplemented with 10mM benzamidine, and stored at −20°C until use. Human VWF antigen levels were determined by ELISA as described before.[24] Samples and a control of normal human plasma were diluted in loading buffer (35mM Tris, 2mM EDTA, 9M urea, 1.2% [weight/volume] SDS, 0.1% [weight/volume] bromophenol blue) to a final concentration of 62.5 ng/mL VWF. VWF multimers were analyzed by 2% (weight/volume) agarose gel electrophoresis followed by Western blot analysis using peroxidase-labeled polyclonal rabbit anti–human VWF antibody (Dako Denmark). Plot profiles of blots were generated with ImageJ software (National Institutes of Health; www.rsb.info.nih.gov/ij, 1997-2009).

Purification of recombinant FVIII

HEK293 cells were grown in DMEM-F12 medium supplemented with 10% FCS. Stable cell lines of HEK293 expressing FVIII-YFP or FVIII-YFP Y1680F were produced as described before.[32] Purification of recombinant FVIII by immunoaffinity chromatography with human antibody VK34[33] (directed against the FVIII heavy chain) has been described previously.[34] Protein concentration was determined by the method of Bradford.[35] FVIII concentration was determined by ELISA essentially as described.[36] Activity of FVIII was determined with a chromogenic assay according to the manufacturer's instructions (Chromogenix). Purified FVIII preparations were analyzed by 7.5% SDS-PAGE under reduced conditions followed by silver staining.

Live cell imaging of flow experiments

BOECs were grown in collagen-coated flow chambers with EGM-20 medium (EGM-2 medium supplemented with EGM bullet kit and 20%

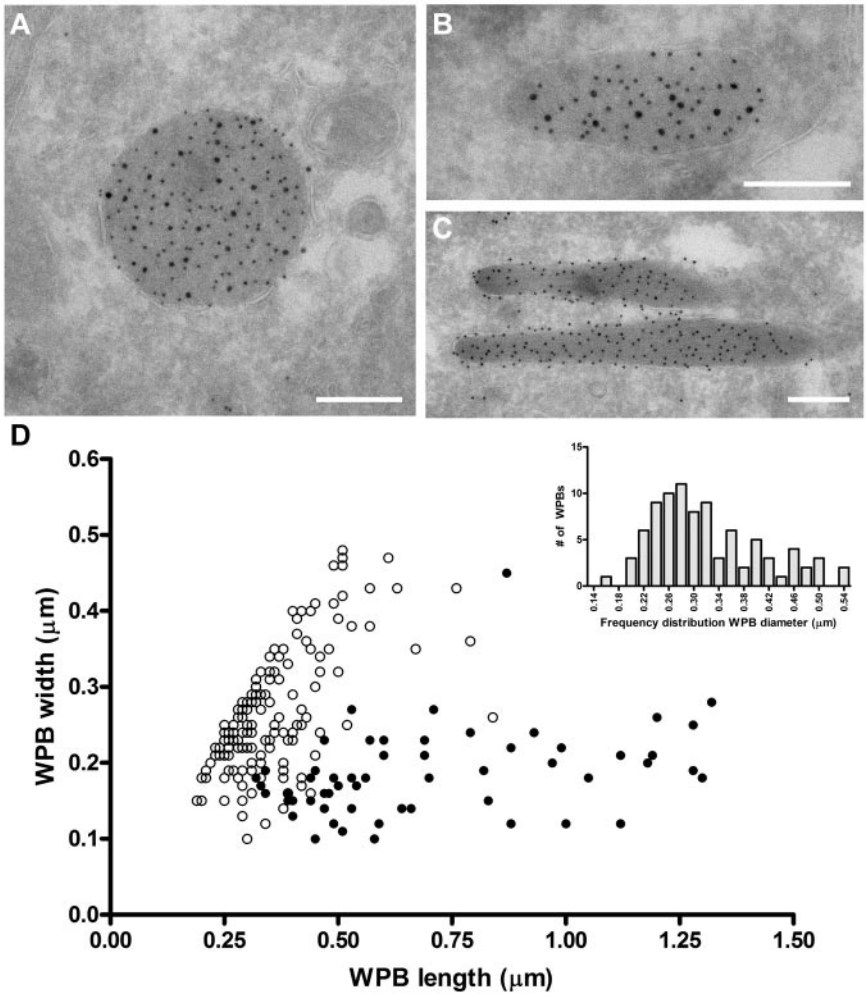

Figure 1. Rounded, electron-dense structures are positive for both FVIII and VWF. (A-C) TEM views of immunogold-labeled WPBs from FVIII-GFP–transduced BOECs, double-labeled with anti–VWF (10 nm gold), and anti-GFP (15 nm gold) to detect FVIII-GFP. Scale bars represent 200 nm. (A) WPBs positive for VWF and FVIII mostly had a rounded morphology. (B) Intermediate, "pear"-shaped WPBs containing both FVIII and VWF. (C) Elongated WPBs are only positive for VWF. (D) Size distribution of WPBs found in nontransduced and FVIII-transduced BOECs. FVIII-negative WPBs (●) had an average length and width of 701 ± 29 nm and 186 ± 58 nm (mean ± SD), respectively. On the other hand, FVIII-positive WPBs (○) were 360 ± 111 nm by 269 ± 81 nm (mean ± SD). Data includes both round and intermediate shaped FVIII-positive WPBs. (Inset) Diameter range of 88 selected FVIII-containing WPBs from panel D that were truly round.

FCS). SF medium supplemented with 100μM histamine was perfused over the cells at 2.5 dyne/cm^2 for 10 minutes. SF medium containing 200 × 10^9 washed human platelets/L, SF medium supplemented with 5 U/mL purified FVIII-YFP or 5 U/mL FVIII-YFP Y1680F was perfused over the cells at the same shear rate. Live-cell imaging was performed at 37°C on a confocal laser scanning microscope using a Zeiss LSM510 equipped with Plan NeoFluar 40×/1.3 oil objective (Carl Zeiss). Images were taken using Zen 2008 LE Version 5.0.0.267 software (Carl Zeiss) at 10-second intervals for indicated time ranges after the onset of perfusion with histamine, unless indicated otherwise. For quantifying the length of VWF strings and the number of platelets on strings, tile scans were made of 1591 × 1591 μm. Images were processed and analyzed with ImageJ software (National Institutes of Health; www.rsb.info.nih.gov/ij, 1997-2009). The number of platelets per micrometer VWF string and length of released strings were determined of at least 30 strings each. Differences between nontransduced and FVIII-transduced BOECs were evaluated by 2-tailed Student *t* test using GraphPad Prism Version 4.03 (GraphPad Software). A value of *P* less than .05 was considered statistically significant.

Immunofluorescent analysis of flow experiments

Confluent BOECs grown in collagen-coated flow chambers were stimulated with SF medium supplemented with 100μM histamine by perfusion at 2.5 dyne/cm^2 for 2 minutes followed by static incubation for 6 minutes, after which flow was continued for an additional 2 minutes. When indicated, cells were perfused with SF medium supplemented with purified FVIII-YFP or FVIII-YFP Y1680F at 5 U/mL for 5 minutes. Cells were washed with PBS at 2.5 dyne/cm^2 for 1 minute and fixed with 3.7% PFA by incubating 2 minutes under flow, 6 minutes under static conditions, and 2 minutes under flow. Cells were washed with PBS and incubated for 1 hour with rabbit anti–human VWF antibody (Dako Denmark) and FITC-labeled CLB-CAg9[37] (directed against FVIII heavy chain) in PBS, 1% BSA. Alexa-633 conjugated antibody was used as secondary antibody to detect VWF. Cells were mounted in Mowiol 4-88 and stored at 4°C until use. Cells were viewed on a Zeiss LSM510 equipped with Plan NeoFluar 40×/1.3 oil objective (Carl Zeiss). All experiments were performed at 37°C.

Results

FVIII affects WPB morphology and VWF tubulation

The ability of VWF to assemble into tubules drives the elongation of endothelial cell-specific WPBs. Previously, we have used confocal microscopy to show that FVIII-containing WPBs display a rounded morphology.[24,25] We now used electron microscopy to study the effect of FVIII on WPB morphology in more detail. Analysis of immunogold-labeled cryosections of an 80% FVIII-positive cell population for VWF and GFP (to detect FVIII-GFP) showed that FVIII was found within large, rounded vesicles (Figure 1A). These structures were always labeled for VWF, which confirms that the rounded structures were indeed WPBs. We also found structures that contained both VWF and FVIII, which were neither rounded nor elongated but intermediate (Figure 1B). In contrast, elongated structures originating from the FVIII-negative subpopulation were only positive for VWF and represented normal

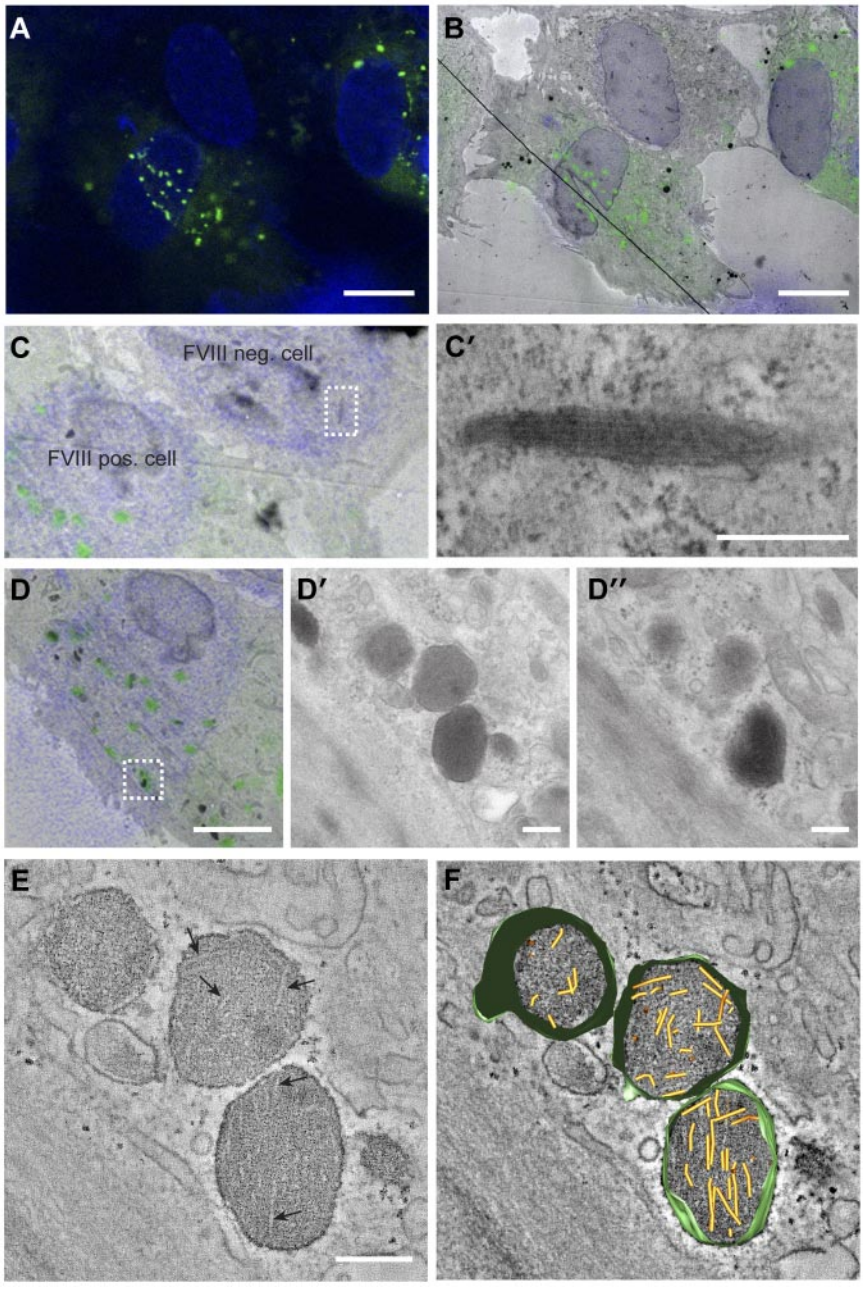

Figure 2. Correlation of FVIII-positive WPBs with rounded, electron-dense structures containing short VWF tubules. (A) Fluorescence image of BOECs expressing FVIII-GFP showing FVIII fluorescence in green and 4,6-diamidino-2-phenylindole staining in blue. Scale bar represents 10 μm. (B) Overlay of transmission electron micrograph and the fluorescence image of the cells shown in panel A. The black line crossing the image represents a fold in the section. Scale bar represents 10 μm. (C) Zoom of panel B showing a FVIII negative and positive BOECs. (C′) Higher magnification TEM view of the boxed area in panel C showing an elongated WPB that does not contain FVIII. Scale bar represents 250 nm. (D) FVIII-positive structures correlating with FVIII-GFP fluorescence. Scale bar represents 4 μm. (D′-D″) Two consecutive sections of the structures boxed in overlay D. Scale bar represents 250 nm. (E) Digital slice through an electron tomogram of the electron-dense structures shown in D-D″ showing FVIII-positive, electron-dense structures with disorganized, short VWF tubules. Arrows indicate longitudinal sections of VWF tubules. Scale bar represents 250 nm. (F) Three-dimensional model of tomogram shown in panel E (see also supplemental Video 1, available on the *Blood* Web site; see the Supplemental Materials link at the top of the online article). Yellow represents VWF tubules; and green, vesicle membranes.

WPBs (Figure 1C). Moreover, we observed that FVIII was randomly distributed throughout WPBs in most cases and did not localize in specific areas in the WPBs (eg, at the vesicle membrane). To quantify the size of FVIII-containing WPBs, we measured the dimensions of 150 randomly selected WPBs (Figure 1D). From this dataset, it appeared that the majority of the measured FVIII-containing WPBs had similar length and width, suggesting a rounded shape. To determine the diameter range of rounded FVIII-containing WPBs, we first defined the dimensions of spherical WPBs using the criterion that a rounded WPB had a length of less than 1.5 times the width. Second, we only measured WPB whose membrane was visible to exclude measurements taken from WPBs that were sectioned at their far ends. Using these 2 criteria, we found that the diameter range of rounded FVIII-containing WPBs is 170 to 540 nm with a median value of 300 nm (Figure 1D inset), which, when considering the estimated section thickness of 90 nm and using the theoretical solution proposed by Parsons et al,[38] gives a corrected value of 380 nm. This was approximately 1.5-fold wider than a cross-sectioned WPB that did not contain FVIII (100-450 nm with a corrected median of 230 nm). We established previously that untagged FVIII also changes the WPB morphology from an elongated to a rounded shape, identical to YFP-tagged FVIII.[25] This eliminates the possibility that the change in morphology is because of the YFP-tag rather than to FVIII storage. These findings confirm at the ultrastructural level that FVIII-containing WPBs display a rounded morphology.

The change in WPB morphology caused by storage of FVIII may indicate that VWF tubule formation is prohibited. We used CLEM to determine whether VWF tubules are present in FVIII-containing WPBs. CLEM allows for the identification of subcellular structures at electron microscopic level that were initially observed by fluorescence microscopy. In Figure 2A through B, 3 endothelial cells are displayed, 2 of which express FVIII in rounded vesicles that are dispersed throughout the cells, whereas

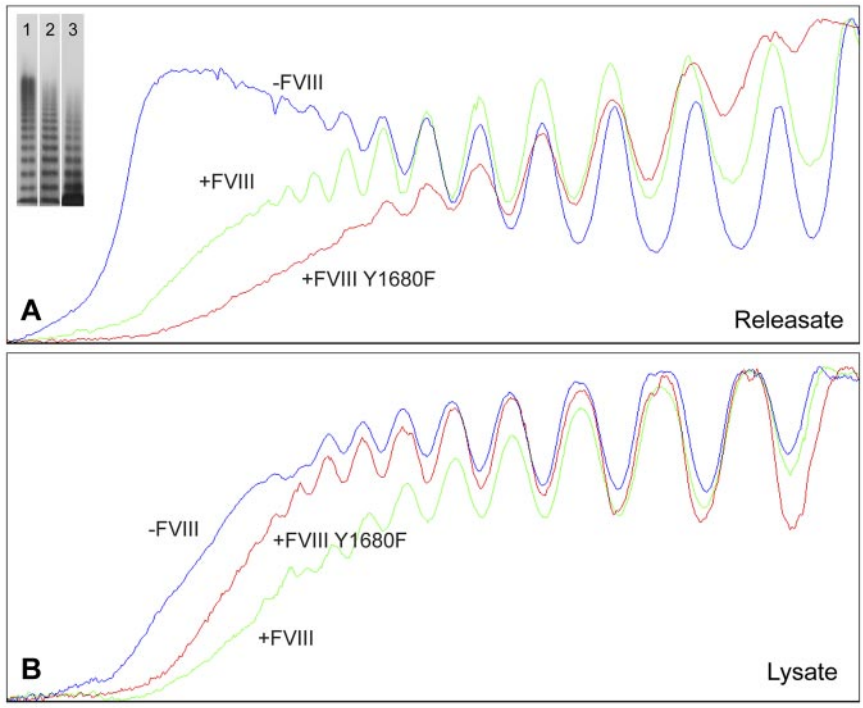

Figure 3. Multimer size of VWF secreted by nontransduced, FVIII-YFP-, and FVIII-YFP Y1680F-transduced BOECs. Plot profiles of VWF multimer patterns of phorbol 12-myristate 13-acetate-induced releasate (A) and lysate of unstimulated cells (B) from nontransduced (lane 1), normal FVIII-YFP (lane 2), and FVIII-YFP Y1680F (lane 3) transduced BOECs. Multimers were analyzed by 2% agarose gel electrophoresis followed by Western blot analysis using rabbit polyclonal anti–human VWF antibody. Plot profiles of blots were generated with ImageJ Software Version 1.44 (National Institutes of Health; www.rsb.info.nih.gov/ij, 1997-2009).

the third cell does not contain these FVIII-positive round vesicles. This FVIII-negative cell displayed the typical cigar-shaped WPBs containing long VWF tubules (Figure 2C-C′). This excludes the possibility of a defective VWF storage system in the cultured BOECs. Tubule-like structures were not visible in FVIII-containing WPBs visualized by 2-dimensional TEM (Figure 2D′-D″). However, 3D electron tomography of FVIII-positive structures identified with CLEM revealed the presence of short and disorganized tubules (Figure 2E-F; supplemental Video 1).

FVIII storage affects VWF multimerization

The lack of long VWF tubules in FVIII-containing WPBs suggests that FVIII interferes with expansion of VWF tubules. Previous findings have shown that the amino-terminal D1-D2-D′-D3 domains direct the formation of VWF tubules.[8,10] The same domains have also been implicated in formation of VWF multimers, whereas the D′-D3 region further contains the high-affinity FVIII binding site.[3] This raises the possibility that FVIII, by its association with VWF, interferes with the process of VWF multimerization. This issue was addressed by comparing VWF multimer patterns from nontransduced and FVIII-transduced BOECs. To assess the contribution of high-affinity FVIII-VWF interaction, we also examined BOECs transduced with FVIII carrying the Y1680F substitution. This variant effectively targets to WPB in HUVECs, despite its strongly reduced affinity for VWF.[16,26] Confocal microscopy revealed that FVIII Y1680F-containing WPBs displayed the typical rounded morphology (supplemental Figure 1). As previously established, FVIII expression in BOECs does not appreciably affect VWF biosynthesis and regulated secretion.[24] Multimer patterns represent VWF released from FVIII-expressing cells, as FVIII-YFP-transduced BOECs were approximately 70% positive for FVIII. Because FVIII-YFP Y1680F BOECs were only approximately 45% positive for FVIII after transduction, these cells were sorted by FACS to increase the percentage of positive cells. Confocal microscopy confirmed that almost all cells (~ 90%) were positive for FVIII Y1680F after sorting.

For nontransduced BOECs, agonist-induced WPB exocytosis resulted in release of VWF multimers containing substantially higher multimeric forms (Figure 3A) than found in cell lysate of unstimulated cells (Figure 3B). Apparently, BOEC-derived elongated WPBs are similar to those from HUVECs in that they contain the ultra-large high molecular weight (UL-HMW) multimers that are lacking in VWF from the constitutive secretion pathway.[6,39] In contrast, VWF from FVIII-containing, rounded WPBs was lacking the highest molecular weight forms (Figure 3A). Interestingly, the multimeric patterns from WPBs containing normal FVIII-YFP and FVIII-YFP Y1680F both show a deficit in UL-HMW multimers (Figure 3A). This suggests that FVIII interferes with multimerization by a mechanism that does not require the high-affinity interaction involving tyrosine 1680. In cell lysates, however, the multimeric patterns from unstimulated nontransduced and FVIII-transduced BOECs were more similar, although the VWF from nontransduced cells tended to display somewhat higher multimerization (Figure 3B). The releasate of FVIII-YFP–transduced cells contained slightly more UL-HMW VWF multimers than releasate from FVIII-YFP Y1680F-transduced BOECs, whereas the reverse was seen in cell lysates (Figure 3A-B). Subtle differences in confluence of the BOECs could be responsible as less confluent cells would hold fewer mature WPBs and therefore contain a slightly lower proportion of UL-HMW multimers.

FVIII has recently been proposed to act as a cofactor for cleavage of VWF strings by ADAMTS13.[40] The multimer patterns of cell lysates (Figure 3B) do not reflect any apparent ADAMTS13-mediated cleavage. Moreover, we were unable to detect any appreciable amounts of ADAMTS13 in BOECs by immunologic methods (data not shown). Therefore, the absence of UL-HMW multimers in VWF secreted by FVIII-expressing cells is unlikely to be the result of increased cleavage by ADAMTS13 during exocytosis. We conclude that in rounded WPBs the UL-HMW multimers are lacking because of interference of FVIII in VWF multimerization.

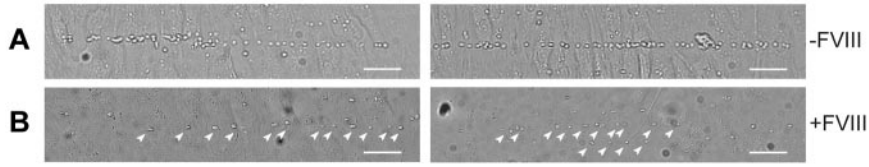

Figure 4. VWF strings released from FVIII-containing WPBs show reduced platelet binding properties. Two images of nontransduced (A) and FVIII-GFP-transduced (B) BOECs stimulated with 100μM histamine at 2.5 dyne/cm^2 for 10 minutes and subsequently perfused with washed human platelets for 5 minutes. Platelet binding to VWF strings originating from nontransduced BOECs is more pronounced than platelet binding to strings released from FVIII-expressing BOECs. Scale bars represent 100 μm. Arrowheads indicate platelets bound to VWF strings released by FVIII-GFP-transduced BOECs. Images were taken on a confocal laser scanning microscopy using a Zeiss LSM510 equipped with Plan NeoFluar 40×/1.3 oil objective (Carl Zeiss) at 37°C.

Rounded FVIII-containing WPB release UL-VWF strings covered with FVIII

The absence of long VWF tubules in FVIII-containing WPBs raised the question of whether FVIII-transduced BOECs could still release UL-VWF strings. UL-VWF strings play a key role in bleeding arrest as platelets adhere to released VWF strings, which ultimately leads to formation of a platelet plug. We examined the ability of FVIII-positive cells to release VWF strings by monitoring platelet adhesion to strings as described previously.[12,41] After stimulation with histamine, nontransduced BOECs released VWF strings that were readily visualized after addition of platelets (Figure 4A; supplemental Video 2). Unexpectedly, VWF strings released from cells expressing FVIII were more difficult to detect as platelet binding was strongly reduced. Closer inspection revealed the presence of sparsely distributed platelets that were arranged in a linear fashion on the surface of FVIII-expressing BOECs (Figure 4B arrowheads). We used live-cell confocal imaging to monitor formation of UL-VWF strings from FVIII-expressing BOECs. Similar to nontransduced BOECs (supplemental Video 2), cells expressing FVIII were able to form VWF strings (supplemental Video 3), but adhesion of platelets to VWF strings derived of FVIII-positive BOECs was strongly reduced compared with that of nontransduced cells. These observations show that the short disorganized VWF tubules still contribute to formation of VWF strings by FVIII-expressing BOECs but that these strings lack the ability to effectively bind platelets.

The presence of FVIII-GFP in rounded WPBs allowed us to monitor release of these organelles in real-time. After stimulation with histamine, FVIII-containing WPBs fused with the plasma membrane and patches of released FVIII were observed from which fluorescent strings emanated (Figure 5A arrowheads). Released UL-VWF strings remained covered with FVIII throughout the entire experiment (15 minutes). Next, we addressed the question as to whether FVIII needs to be in complex with VWF inside WPBs to bind to VWF strings. Nontransduced BOECs were stimulated with histamine followed by perfusion with purified FVIII-YFP to determine whether exogenous FVIII is able to bind to VWF strings under flow. It is to be noted that we previously

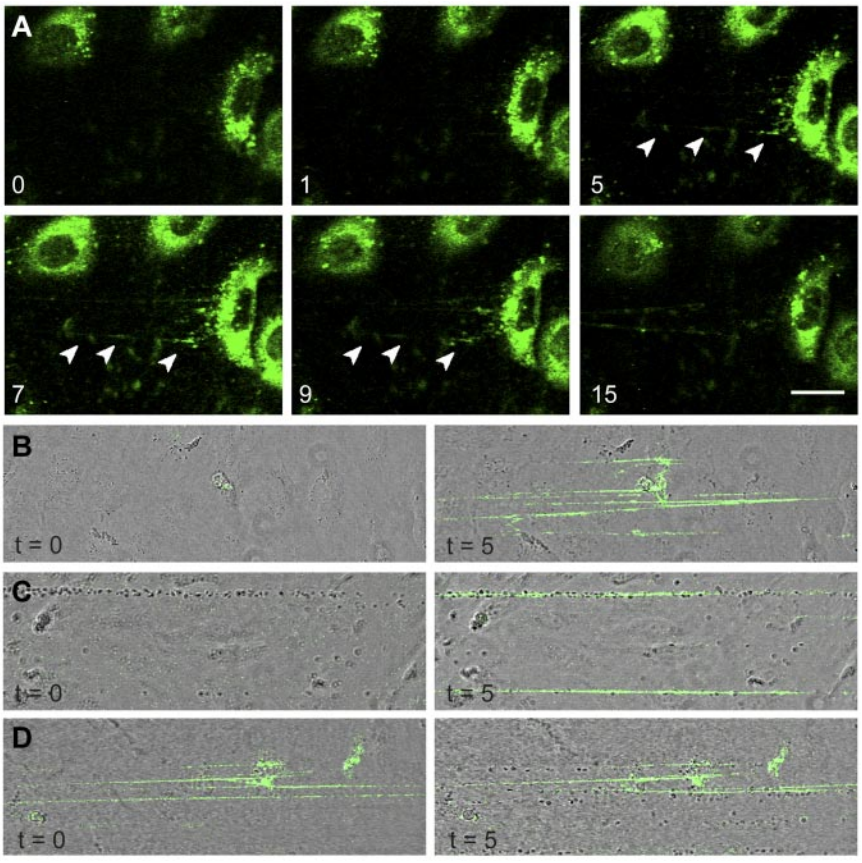

Figure 5. FVIII-containing, rounded WPBs release UL-VWF strings covered with FVIII. (A) FVIII-GFP–transduced BOECs were stimulated with 100μM histamine at 2.5 dyne/cm^2. Shown are fluorescent images taken at indicated time points (in minutes) after the onset of flow. Green represents FVIII fluorescence. Arrowheads indicate released patches and strings. Scale bar represents 20 μm. (B) Nontransduced BOECs were stimulated with 100μM histamine at 2.5 dyne/cm^2 for 10 minutes to stimulate exocytosis of WPBs and subsequently incubated with 5 U/mL purified FVIII-YFP for 5 minutes. Images were taken at the indicated time points (in minutes) after the onset of FVIII-YFP perfusion. (C) Nontransduced BOECs were stimulated with 100μM histamine at 2.5 dyne/cm^2 for 10 minutes and subsequently incubated with washed platelets for 5 minutes before addition of 5 U/mL purified FVIII-YFP for 5 minutes. (D) Nontransduced BOECs were stimulated with 100μM histamine at 2.5 dyne/cm^2 for 10 minutes, incubated with 5 U/mL purified FVIII-YFP for 5 minutes, followed by perfusion of washed human platelets for 5 minutes. Live-cell imaging was performed at 37°C on a confocal laser scanning microscopy using a Zeiss LSM510 equipped with Plan NeoFluar 40×/1.3 oil objective (Carl Zeiss) at 37°C.

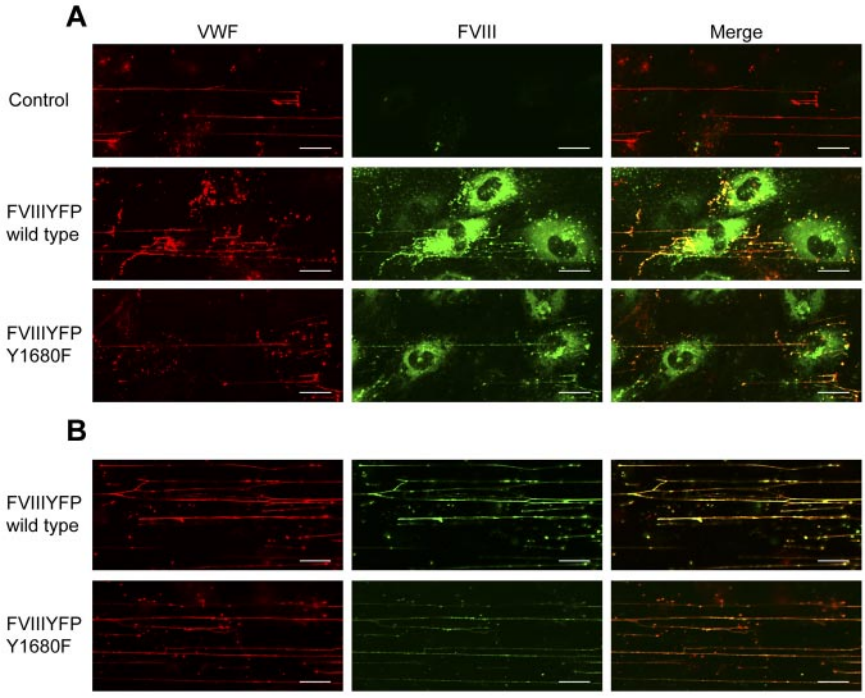

Figure 6. FVIII Y1680F variant binds to VWF strings when expressed by BOECs or exogenously added. (A) Nontransduced, FVIII-YFP-, and FVIII-YFP Y1680F-transduced BOECs were stimulated with 100μM histamine at 2.5 dyne/cm^2, fixed and stained for VWF (red) and FVIII (green). (B) Nontransduced BOECs were stimulated with 100μM histamine at 2.5 dyne/cm^2 followed by perfusion with 5 U/mL purified FVIII-YFP or 5 U/mL FVIII-YFP Y1680F. Cells were fixed and stained for VWF (red) and FVIII (green). Scale bars represent 20 μm.

established that the YFP-tag in FVIII does not interfere with FVIII binding to VWF.[26] Exogenous FVIII was capable of binding to UL-VWF strings without precomplexation in WPBs (Figure 5B). In addition, exogenous FVIII was also able to bind to VWF strings that were already covered with platelets (Figure 5C). Surprisingly, whereas endogenous FVIII interfered with platelet binding (Figure 4B), VWF strings covered with exogenous FVIII did display platelet binding (Figure 5D). This shows that newly released UL-VWF strings have the capacity to recruit both platelets and exogenous FVIII.

FVIII Y1680F remains associated with released VWF strings

The observation that WPB-derived FVIII, but not exogenous FVIII, effectively reduces platelet binding suggests a difference in FVIII binding to VWF strings, for instance, in terms of affinity. This issue was addressed by flow experiments using the FVIII-YFP Y1680F variant. Although we intended to use the YFP-tag for detection of FVIII, the fluorescent signal of the YFP-tag proved too weak to detect FVIII outside the WPBs. Therefore, we used FITC-labeled antibodies to detect extracellular FVIII. Because of its strongly reduced affinity for VWF,[30] we anticipated that FVIII-YFP Y1680F released from BOECs would not bind to VWF strings or dissociate quickly after exocytosis. FVIII-YFP Y1680F released by endothelial cells remained detectable on VWF strings, however, and the fluorescence intensity was similar to that of strings covered with normal FVIII (Figure 6A). To determine whether binding of FVIII to strings is dependent on FVIII-VWF costorage in WPBs, purified FVIII-YFP Y1680F was perfused over histamine-treated BOECs. Exogenously added FVIII Y1680F did bind to VWF strings, but the intensity of the FVIII fluorescent signal was slightly reduced compared with exogenously added normal FVIII (Figure 6B). This finding suggests that, in contrast to "endogenous" FVIII from WPBs, binding of exogenous FVIII to VWF strings may be more dependent on high-affinity, tyrosine 1680-mediated interaction with VWF. However, because our data are purely qualitative, additional quantitative research is needed to address possible differences in endogenous and exogenous FVIII binding to VWF strings.

VWF strings released from FVIII-expressing endothelial cells bind fewer platelets

The relation between FVIII binding and platelet recruitment to VWF strings was further explored using a quantitative approach. First, we determined the length of FVIII-covered strings and compared this with the length of strings released from nontransduced BOECs. We found that, despite their shorter tubules, FVIII-covered strings were of similar length as VWF strings secreted by nontransduced BOECs, on average 338 μm and 360 μm, respectively (Figure 7A). Strings released from cells expressing FVIII Y1680F were slightly shorter (average, 297 μm), although this difference was not statistically significant. The length of VWF strings ranged from approximately 160 to 830 μm for nontransduced BOECs, approximately 170 to 600 μm for FVIII-transduced, and approximately 125 to 930 μm for FVIII Y1680F-transduced BOECs. We then calculated the number of platelets bound per micrometer VWF string. FVIII-covered strings were able to bind an average number of 0.07 platelets per micrometer string, whereas normal VWF strings contained on average 0.18 platelets per micrometer string (Figure 7B). In other words, a typical FVIII-covered string of 338 μm can bind 24 platelets, whereas non–FVIII-covered strings recruit 65 platelets. Surprisingly, VWF strings released from FVIII Y1680F-positive cells displayed an intermediate defect in platelet binding as strings bound on average 0.11 platelets per micrometer string. These quantitative data are fully compatible with our qualitative observations (Figures 4-6) and raise the possibility that the presence of WPB-derived FVIII on VWF strings impairs platelet recruitment. In contrast, the presence of exogenous FVIII did not interfere with platelet binding to any appreciable extent (Figure 7C).

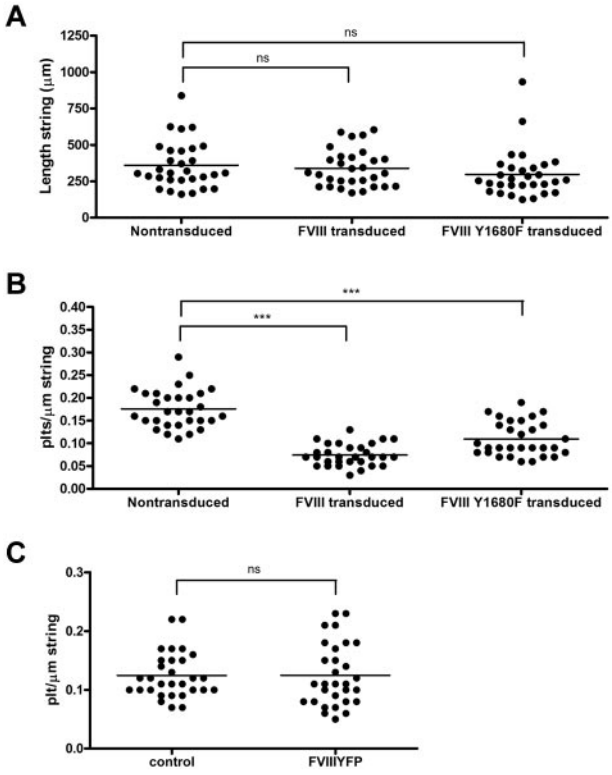

Figure 7. Quantification of platelet binding properties and length of VWF strings from FVIII-YFP and FVIII-YFP Y1680F-transduced BOECs. Fluorescence and phase-contrast tile scans were used to measure length of released VWF strings (A) and number of platelets per string (B) of at least 30 strings each from nontransduced, normal FVIII-YFP-, and FVIII-YFP Y1680F-transduced BOECs. (A) No significant differences were detected in the length of VWF strings released by nontransduced BOECs, FVIII-YFP-, and FVIII-YFP Y1680F-transduced BOECs, 360 ± 29 μm, 338 ± 23 μm ($P = .57$), and 297 ± 30 μm ($P = .14$), respectively. Values are mean ± SD. ns indicates not significant. (B) VWF strings released by FVIII-YFP- and FVIII-YFP Y1680F-transduced BOECs bind fewer platelets than strings released by nontransduced BOECs, 0.07 ± 0.02, 0.11 ± 0.04, and 0.18 ± 0.04, respectively (mean ± SD). ***$P < .001$. (C) Nontransduced BOECs were stimulated with 100μM histamine at 2.5 dyne/cm^2 for 10 minutes, incubated with SF medium (control) or 5 U/mL purified FVIII-YFP for 5 minutes followed by perfusion of washed human platelets for 5 minutes. Number of platelets per string was determined of 30 strings each. No difference was observed in platelet binding between strings covered with or without recombinant FVIII ($P = .98$).

Discussion

Although vascular endothelial cells in general are devoid of FVIII biosynthesis, recent evidence suggests the existence of specific subsets that do synthesize FVIII and store FVIII together with VWF in WPB-like storage organelles.[19-22] The regulated FVIII secretion observed from these cells may represent the FVIII storage pool that is released in vivo on administration of the vasopressin analog desmopressin[22] and, as such, adds physiologic significance to endothelial FVIII expression. In the present study, we have used BOECs to study the implications of FVIII overexpression in endothelial cells. We observed that FVIII overexpression causes a variety of changes, including the size and organization of VWF tubules in WPBs (Figures 1 and 2), the size of the VWF multimers (Figure 3), and the recruitment of platelets to VWF strings once released from WPBs (Figures 4-7).

With regard to WBP morphology, it has been well established that VWF is stored in WPBs as helical tubules that provide these organelles with their typical elongated shape. Tubule formation occurs in the TGN where acidic pH and high Ca^{2+} concentrations promote binding of propeptide D1-D2 to the D′-D3 domains.[8] In the same compartment, propeptide is cleaved from mature VWF, most likely by furin.[42,43] The propeptide remains noncovalently associated with D′-D3 domains, thereby stabilizing the helical conformation of VWF tubules.[8,10] We observed that FVIII targeting to WPBs disrupts the parallel alignment and compaction of VWF tubules into elongated WPBs (Figures 1 and 2). Possibly, FVIII may interfere with propeptide binding to the VWF D′-D3 domains, thereby preventing the extension of VWF tubules and the resulting elongation of WPBs. We have previously established that the molar ratio of FVIII to VWF in WPBs of FVIII-transduced BOECs is on average 1:15.[24] The relatively low amount of FVIII compared with VWF might explain why VWF tubulation is only partially impaired by FVIII. Our data seem compatible with a model in which FVIII blocks binding of propeptide during covalent addition of VWF multimers to the growing tubule.

With regard to tubule length, Huang et al reported that helical tubules created in vitro from propeptide and D′-D3 dimers contain 4.2 dimers per turn, with one helix segment spanning 11 nm.[8] Accordingly, a 5 μm measuring WPB with VWF tubules spanning the entire length has tubules containing approximately 3800 VWF subunits and a mass of approximately 975 million Da. This corresponds with an extended length of 250 μm, which is compatible with the length of a VWF string.[8,13] In our study (Figure 1), most FVIII-containing WPBs measure approximately 380 nm in diameter and do not contain tubules spanning the entire WPBs. In line with the aforementioned calculations, these organelles should release strings no longer than approximately 19 μm. Our data show that FVIII-expressing endothelial cells release strings that are much longer, with an average length of 340 μm (Figure 7A). This argues in favor of linkage of VWF multimers after release[44,45] or pooling of WPB content during multigranular exocytosis.[28] Moreover, tubular organization of VWF appears dispensable for the formation of UL-VWF string on the surface of endothelial cells.

Despite their normal length, VWF strings from FVIII-expressing cells display greatly reduced platelet recruitment (Figures 4 and 7B). Indeed, it was even more reduced than reported for monensin-treated cells, which completely lack VWF tubules.[10] This suggests that the reduction in platelet binding is not related to the decreased tubule length in these cells but to the presence of FVIII. Indeed, we could visualize WPB-derived FVIII on the VWF strings once released (Figure 5). Moreover, VWF strings were capable of recruiting exogenously added FVIII. Nonetheless, it seems not merely the presence of FVIII that interferes with platelet binding. This can be concluded from our qualitative (Figure 5) and quantitative (Figure 7) data demonstrating that the presence of endogenous, but not exogenous, FVIII inhibits platelet binding. This apparent paradox points toward a contribution at the level of intracellular FVIII-VWF assembly. We addressed this issue by assessing the effect of the FVIII Y1680F variant, which lacks the high-affinity interaction with VWF.[16,26] This mutant, however, proved surprisingly similar to normal FVIII. Not only does this variant cotarget with VWF to WPBs,[26] it also induces the rounded WPB morphology (supplemental Figure 1). Moreover, FVIII Y1680F also interferes with formation of the UL-HMW VWF multimers (Figure 3), remains bound to VWF strings from WPBs (Figure 6), and reduces platelet recruitment (Figure 7). These findings suggest that the interaction of FVIII with VWF within and during formation of WPBs differs from that in the circulating FVIII-VWF complex and that after WPB release this difference is maintained on VWF strings.

Infusion with desmopressin typically results in a 2- to 4-fold increase in circulating FVIII levels of healthy persons.[46] Assuming that the human body holds approximately 3 L plasma and 1 unit of FVIII is 0.1 μg, a 2-fold increase in FVIII plasma levels would imply the additional release of 300 μg FVIII from storage pools. We previously reported that, on WPB exocytosis, FVIII overexpressing endothelial cells release approximately 0.5 μg of FVIII per 1×10^6 cells.[24] Therefore, the release of 300 μg would require approximately 600×10^6 FVIII-containing cells (ie, only a fraction of the estimated number of 60×10^{18} endothelial cells in the human body).[47] Even if the actual FVIII secretion is lower, it is obvious that only a small number of endothelial cells needs to store and release appreciable amounts of FVIII. Based on our current findings, it seems reasonable to expect that this subset of endothelial cells differs in VWF storage and in the ability of secreted VWF strings to bind platelets.

Theoretically, the reduction of platelet binding to VWF strings from FVIII-expressing cells may be because of steric hindrance, whereby FVIII shields part of the VWF A1 domain that is involved in platelet binding. Alternatively, the association with FVIII might interfere with the conformational changes in VWF that are needed for exposure of platelet binding sites in the VWF A1 domain.[3,48,49] Simultaneous binding of exogenous FVIII and platelets (Figures 5 and 7C) indicates that intracellular storage of FVIII prohibits the conformational change in VWF or that exogenous and endogenous FVIII associate in a different way with VWF strings. The similarities between normal FVIII and FVIII Y1680F could indicate that intracellular FVIII-VWF assembly involves other molecular sites in FVIII, and possibly also in VWF, in addition to those previously established for these proteins in circulation. This might also explain why VWF variants with reduced FVIII binding in the circulation are still able to target FVIII to WPBs.[25] We therefore propose that structural elements that play a minor role in extracellular FVIII-VWF complex formation do contribute considerably to intracellular assembly of FVIII to VWF.

Acknowledgments

The authors thank J. J. Onderwater for technical assistance with the immunogold labeling experiments, A. M. Mommaas for helpful discussions with the immunogold labeling experiments, and Jack A. Valentijn for helpful discussion and help with the CLEM.

This work was supported by Sanquin Blood Supply Foundation (grant PPOC-07-025) and The Netherlands Organization for Scientific Research NWO (grant TOP91209006).

Authorship

Contribution: E.A.M.B. and M.J.M. performed experiments, analyzed data, made the figures, and wrote the paper; M.v.d.B. and J.C.J.E. designed research and analyzed data; and J.V., K.M.V., and K.M. designed research, analyzed data, and wrote the paper.

Conflict-of-interest disclosure: The authors declare no competing financial interests.

Correspondence: Koen Mertens, Department of Plasma Proteins, Sanquin Research, Plesmanlaan 125, 1066 CX Amsterdam, The Netherlands; e-mail: k.mertens@sanquin.nl.

References

1. Weibel ER, Palade GE. New cytoplasmic components in arterial endothelia. *J Cell Biol.* 1964; 23(1):101-112.
2. Rondaij MG, Bierings R, Kragt A, van Mourik JA, Voorberg J. Dynamics and plasticity of Weibel-Palade bodies in endothelial cells. *Arterioscler Thromb Vasc Biol.* 2006;26(5):1002-1007.
3. Sadler JE. Biochemistry and genetics of von Willebrand Factor. *Annu Rev Biochem.* 1998; 67(1):395.
4. Vischer UM, Wagner DD. von Willebrand factor proteolytic processing and multimerization precede the formation of Weibel-Palade bodies. *Blood.* 1994;83(12):3536-3544.
5. Voorberg J, Fontijn R, Calafat J, Janssen H, van Mourik JA, Pannekoek H. Assembly and routing of von Willebrand factor variants: the requirements for disulfide-linked dimerization reside within the carboxy-terminal 151 amino acids. *J Cell Biol.* 1991;113(1):195-205.
6. Wagner DD. Cell biology of von Willebrand factor. *Annu Rev Cell Biol.* 1990;6(1):217-242.
7. Berriman JA, Li S, Hewlett LJ, et al. Structural organization of Weibel-Palade bodies revealed by cryo-EM of vitrified endothelial cells. *Proc Natl Acad Sci U S A.* 2009;106(41):17407-17412.
8. Huang R-H, Wang Y, Roth R, et al. Assembly of Weibel-Palade body-like tubules from N-terminal domains of von Willebrand factor. *Proc Natl Acad Sci U S A.* 2008;105(2):482-487.
9. Valentijn KM, Valentijn JA, Jansen KA, Koster AJ. A new look at Weibel-Palade body structure in endothelial cells using electron tomography. *J Struct Biol.* 2008;161(3):447-458.
10. Michaux G, Abbitt KB, Collinson LM, Haberichter SL, Norman KE, Cutler DF. The physiological function of von Willebrand's factor depends on its tubular storage in endothelial Weibel-Palade bodies. *Dev Cell.* 2006;10(2):223-232.
11. Andre P, Denis CV, Ware J, et al. Platelets adhere to and translocate on von Willebrand factor presented by endothelium in stimulated veins. *Blood.* 2000;96(10):3322-3328.
12. Dong J-F, Moake JL, Nolasco L, et al. ADAMTS-13 rapidly cleaves newly secreted ultralarge von Willebrand factor multimers on the endothelial surface under flowing conditions. *Blood.* 2002;100(12):4033-4039.
13. Sadler JE. von Willebrand factor assembly and secretion. *J Thromb Haemost.* 2009;7(suppl 1): 24-27.
14. Lenting PJ, van Mourik JA, Mertens K. The life cycle of coagulation factor VIII in view of its structure and function. *Blood.* 1998;92(11):3983-3996.
15. Leyte A, Verbeet MP, Brodniewicz-Proba T, van Mourik JA, Mertens K. The interaction between human blood-coagulation factor VIII and von Willebrand factor: characterization of a high-affinity binding site on factor VIII. *Biochem J.* 1989;257(3):679-683.
16. Leyte A, van Schijndel HB, Niehrs C, et al. Sulfation of Tyr1680 of human blood coagulation factor VIII is essential for the interaction of factor VIII with von Willebrand factor. *J Biol Chem.* 1991; 266(2):740-746.
17. Lamont PA, Ragni MV. Lack of desmopressin (DDAVP) response in men with hemophilia A following liver transplantation. *J Thromb Haemost.* 2005;3(10):2259-2263.
18. Hollestelle MJ, Poyck PPC, Hollestelle JM, Marsman HA, van Mourik JA, Gulik TM. Extrahepatic factor VIII expression in porcine fulminant hepatic failure. *J Thromb Haemost.* 2005;3(10): 2274-2280.
19. Do H, Healey JF, Waller EK, Lollar P. Expression of factor VIII by murine liver sinusoidal endothelial cells. *J Biol Chem.* 1999;274(28):19587-19592.
20. Jacquemin M, Neyrinck A, Hermanns MI, et al. FVIII production by human lung microvascular endothelial cells. *Blood.* 2006;108(2):515-517.
21. Shovlin CL, Angus G, Manning RA, et al. Endothelial cell processing and alternatively spliced transcripts of factor VIII: potential implications for coagulation cascades and pulmonary hypertension. *PLoS One.* 2010;5(2):e9154.
22. Shahani T, Lavend'homme R, Luttun A, Saint-Remy J-M, Peerlinck K, Jacquemin M. Activation of human endothelial cells from specific vascular beds induces the release of a FVIII storage pool. *Blood.* 2010;115(23):4902-4909.
23. Shi Q, Fahs SA, Kuether EL, Cooley BC, Weiler H, Montgomery RR. Targeting FVIII expression to endothelial cells regenerates a releasable pool of FVIII and restores hemostasis in a mouse model of hemophilia A. *Blood.* 2010;116(16):3049-3057.
24. van den Biggelaar M, Bouwens EAM, Kootstra NA, Hebbel RP, Voorberg J, Mertens K. Storage and regulated secretion of factor VIII in blood outgrowth endothelial cells. *Haematologica.* 2009; 94(5):670-678.
25. van den Biggelaar M, Meijer AB, Voorberg J, Mertens K. Intracellular cotrafficking of factor VIII and von Willebrand factor type 2N variants to storage organelles. *Blood.* 2009;113(13):3102-3109.
26. van den Biggelaar M, Bierings R, Storm G, Voorberg J, Mertens K. Requirements for cellular co-trafficking of factor VIII and von Willebrand factor to Weibel-Palade bodies. *J Thromb Haemost.* 2007;5(11):2235-2243.
27. Rosenberg JB, Foster PA, Kaufman RJ, et al. Intracellular trafficking of factor VIII to von Willebrand factor storage granules. *J Clin Invest.* 1998;101(3):613-624.
28. Valentijn KM, van Driel LF, Mourik MJ, et al. Multigranular exocytosis of Weibel-Palade bodies in

vascular endothelial cells. *Blood.* 2010;116(10):1807-1816.

29. Mastronarde DN. Automated electron microscope tomography using robust prediction of specimen movements. *J Struct Biol.* 2005;152(1):36-51.
30. Kremer JR, Mastronarde DN, McIntosh JR. Computer visualization of three-dimensional image data using IMOD. *J Struct Biol.* 1996;116(1):71-76.
31. Watanabe Y, Itoh S, Goto T, et al. TMEPAI, a transmembrane TGF-beta-inducible protein, sequesters Smad proteins from active participation in TGF-beta signaling. *Mol Cell.* 2010;37(1):123-134.
32. Fribourg C, Meijer AB, Mertens K. The interface between the EGF2 domain and the protease domain in blood coagulation factor IX contributes to factor VIII binding and factor X activation. *Biochemistry.* 2006;45(35):10777-10785.
33. van den Brink EN, Turenhout EAM, Bank CMC, Fijnvandraat K, Peters M, Voorberg J. Molecular analysis of human anti–factor VIII antibodies by V gene phage display identifies a new epitope in the acidic region following the A2 domain. *Blood.* 2000;96(2):540-545.
34. Meems H, van den Biggelaar M, Rondaij M, van der Zwaan C, Mertens K, Meijer AB. C1 domain residues Lys 2092 and Phe 2093 are of major importance for the endocytic uptake of coagulation factor VIII. *Int J Biochem Cell Biol.* 2011;43(8):1114-1121.
35. Bradford MM. A rapid and sensitive method for the quantitation of microgram quantities of protein utilizing the principle of protein-dye binding. *Anal Biochem.* 1976;72:248-254.
36. Donath M-JSH, Lenting PJ, van Mourik JA, Mertens K. The role of cleavage of the light chain at positions Arg1689 or Arg1721 in subunit interaction and activation of human blood coagulation factor VIII. *J Biol Chem.* 1995;270(8):3648-3655.
37. Stel HV, Sakariassen KS, Scholte BJ, et al. Characterization of 25 monoclonal antibodies to factor VIII-von Willebrand factor: relationship between ristocetin-induced platelet aggregation and platelet adherence to subendothelium. *Blood.* 1984;63(6):1408-1415.
38. Parsons TD, Coorssen JR, Horstmann H, Almers W. Docked granules, the exocytic burst, and the need for ATP hydrolysis in endocrine cells. *Neuron.* 1995;15(5):1085-1096.
39. Moake JL, Rudy CK, Troll JH, et al. Unusually large plasma factor VIII: von Willebrand factor multimers in chronic relapsing thrombotic thrombocytopenic purpura. *N Engl J Med.* 1982;307(23):1432-1435.
40. Cao W, Krishnaswamy S, Camire RM, Lenting PJ, Zheng XL. Factor VIII accelerates proteolytic cleavage of von Willebrand factor by ADAMTS13. *Proc Natl Acad Sci U S A.* 2008;105(21):7416-7421.
41. Pos W, Crawley JTB, Fijnheer R, Voorberg J, Lane DA, Luken BM. An autoantibody epitope comprising residues R660, Y661, and Y665 in the ADAMTS13 spacer domain identifies a binding site for the A2 domain of VWF. *Blood.* 2010;115(8):1640-1649.
42. van de Ven WJ, Voorberg J, Fontijn R, et al. Furin is a subtilisin-like proprotein processing enzyme in higher eukaryotes. *Mol Biol Rep.* 1990;14(4):265-275.
43. Wise RJ, Barr PJ, Wong PA, Kiefer MC, Brake AJ, Kaufman RJ. Expression of a human proprotein processing enzyme: correct cleavage of the von Willebrand factor precursor at a paired basic amino acid site. *Proc Natl Acad Sci U S A.* 1990;87(23):9378-9382.
44. Li Y, Choi H, Zhou Z, et al. Covalent regulation of ULVWF string formation and elongation on endothelial cells under flow conditions. *J Thromb Haemost.* 2008;6(7):1135-1143.
45. Savage B, Sixma JJ, Ruggeri ZM. Functional self-association of von Willebrand factor during platelet adhesion under flow. *Proc Natl Acad Sci U S A.* 2002;99(1):425-430.
46. Mannucci PM, Canciani MT, Rota L, Donovan BS. Response of factor VIII/von Willebrand factor to DDAVP in healthy subjects and patients with haemophilia A and von Willebrand's disease. *Br J Haematol.* 1981;47(2):283-293.
47. Aird WC. Phenotypic heterogeneity of the endothelium: I. Structure, function, and mechanisms. *Circ Res.* 2007;100(2):158-173.
48. Hulstein JJ, de Groot PG, Silence K, Veyradier A, Fijnheer R, Lenting PJ. A novel nanobody that detects the gain-of-function phenotype of von Willebrand factor in ADAMTS13 deficiency and von Willebrand disease type 2B. *Blood.* 2005;106(9):3035-3042.
49. Sadler JE. New concepts in von Willebrand disease. *Annu Rev Med.* 2005;56(1):173-191.